Molecular Therapy
Nucleic Acids
Original Article

Liposome-mediated small RNA delivery to convert the macrophage polarity: A novel therapeutic approach to treat inflammatory uterine disease

Mira Park,[1,4] Hyeon-Ji Oh,[2,4] Jieun Han,[2] Seok-Ho Hong,[3] Wooram Park,[2] and Haengseok Song[1]

[1]Department of Biomedical Science, CHA University, 335 Pangyo-ro, Bundang-gu, Seongnam, Gyeonggi 13488, Republic of Korea; [2]Department of Integrative Biotechnology, College of Biotechnology and Bioengineering, Sungkyunkwan University, Seoburo 2066, Suwon, Gyeonggi 16419, Republic of Korea; [3]Department of Internal Medicine, Kangwon National University, Chuncheon, Kangwon 24341, Republic of Korea

Macrophages are present in all tissues for maintaining tissue homeostasis, and macrophage polarization plays a vital role in alleviating inflammation. Therefore, specific delivery of polarization modulators to macrophages *in situ* is critical for treating inflammatory diseases. We demonstrate that a size-controlled miRNA-encapsulated macrophage-targeting liposomes (miR/MT-Lip) specifically targets macrophages to promote M1-to-M2 polarization conversion, alleviating inflammation without cytotoxicity. miR/MT-Lip, approximately 1.2 μm, showed excellent internalization through phagocytosis and/or macropinocytosis in macrophages. miR-10a/MT-Lip, but not scramble miR-Fluorescein amidite (FAM)/MT-Lip as control, effectively converted the polarization of lipopolysaccharide (LPS)-induced M1 macrophages to M2 *in vitro*. When miR-10a/MT-Lip was intravenously delivered to mice insulted with LPS for inflammation, the proportion of M2 macrophages was significantly increased without disturbing the population of other immune cells. Furthermore, scramble miR-FAM/MT-Lip was mainly detected in macrophages, but not other immune cells. When our miR/MT-Lip was administered to mice with Asherman's syndrome that suffer from infertility because of sterile uterine inflammation, macrophage-specific targeting of miR-10a/MT-Lip facilitated M1-to-M2 conversion for angiogenesis in the impaired uterus, resulting in restoration of healthy uterine conditions. The results indicate that our MT-Lip encapsulating small RNAs has excellent potential to treat various inflammatory disorders by fine-tuning macrophage polarization *in vivo* without any side effects.

INTRODUCTION

Inflammation is a complex biological response of the immune system to harmful pathogens.[1,2] In maintaining immune homeostasis, acute inflammatory responses play essential roles in the innate immune system as defense mechanisms. However, excessive activation of immune cells and prolonged acute inflammatory response cause chronic inflammation, resulting in tissue damage.[3] Chronic inflammation is responsible for various diseases, such as cancer, arthritis, asthma, diabetes, arteriosclerosis, inflammatory bowel disease (IBD), and Asherman's syndrome (AS).[4–6] AS is a complex gynecological disorder characterized by intrauterine adhesions or fibrosis resulting from the destruction of the basal layer of the endometrium,[7] where endometrial stem/progenitor cells are believed to reside.[8] Patients with AS suffer from recurrent pregnancy loss, amenorrhea, hypomenorrhea, and placental abnormalities, leading to infertility.[9] Mesenchymal stem cells (MSCs) from various tissues have been applied to restore the function of impaired endometrium in patients and animal models with AS, although critical drawbacks, such as long-term safety, immunogenicity, and heterogeneity, remain unsolved.[10] MSCs can interact with various immune cells, including monocytes and macrophages, to produce anti-inflammatory effects under a specific microenvironment.[11] Thus, modulating the function of these immune cells with functional plasticity has great potential to ameliorate inflammatory milieu in the endometrium with AS, and the development of biological platforms to modulate the immune cell plasticity *in vivo* is strongly needed.

Macrophages play a key role in maintaining tissue homeostasis and are also active actors during infection, autoimmunity, inflammation, and cancer.[12] Macrophages show a wide spectrum of plasticity from classically activated M1 (pro-inflammatory) to alternatively activated M2 (anti-inflammatory), depending on the microenvironment.[13] Thus, the M1/M2 ratio is more informative to demonstrate the polarization status of macrophages because it is "fluid," which explains that macrophage phenotypes can be dynamically fine-tuned in tissues.[14] Inflammation persistence is partially due to a high M1/M2 macrophage ratio.[15] In inflamed tissues, monocytes are differentiated into M1 macrophages and promote inflammation by releasing inflammatory cytokines, reactive oxygen species, and proteases.[16] Anti-inflammatory cytokines such as interleukin-4 (IL-4) have been used in the M2

Received 15 July 2022; accepted 17 November 2022;
https://doi.org/10.1016/j.omtn.2022.11.018.

[4]These authors contributed equally

Correspondence: Wooram Park, PhD, Department of Integrative Biotechnology, College of Biotechnology and Bioengineering, Sungkyunkwan University, Seoburo 2066, Suwon, Gyeonggi 16419, Republic of Korea.
E-mail: parkwr@skku.edu
Correspondence: Haengseok Song, PhD, Department of Biomedical Science, CHA University, 335 Pangyo-ro, Bundang-gu, Seongnam, Gyeonggi 13488, Republic of Korea.
E-mail: hssong@cha.ac.kr

polarization of macrophages to treat various inflammatory diseases.[17] However, repeated injection of high doses of anti-inflammatory cytokines with a short half-life causes systemic side effects.[18] MicroRNAs (miRNAs), non-coding endogenous ribonucleic acid strands 20–24 nt in length, bind to the 3′ untranslated regions of the target mRNA for post-transcriptional regulation of gene expression.[19] Findings that miRNAs regulate inflammation through macrophage M2 polarization[20,21] show the potential of miRNAs as therapeutic agents for inflammation. However, naked miRNA has limitations in clinical application because it is rapidly degraded or inactivated by nucleases in the bloodstream and has undesired off-target effects.[22]

Recent work has pursued various nanotechnology strategies for precisely targeting macrophages to reduce inflammation by altering polarization.[23–26] Such nanoparticles increase the *in vivo* half-life of anti-inflammatory agents (e.g., cytokines and miRNA) and enable macrophage-specific delivery.[27,28] Nanoparticles modified with macrophage-specific ligands can effectively deliver M2 polarization inducers to macrophages. It is also possible to target macrophages through the control of nanoparticle size because the macrophage internalization mechanism is phagocytosis dependent. It has been reported that macrophages effectively phagocytose particles larger than 500 nm.[29,30] Clodronate-encapsulated liposomes 1.5–2.0 μm in size can eliminate 80%–90% of splenic macrophages with a single administration at the cellular and whole-animal levels.[31,32] Thus, in this study, we produced a functional miRNA-encapsulated liposome with controlled particle size to specifically target macrophages (MT-Lips). We encapsulate miR-10a, a miRNA known to induce M2 polarization of macrophages,[33] in MT-Lip as miR-10a/MT-Lip and demonstrate an effective increase in the proportion of M2-polarized macrophages without disturbing the population of other immune cells. This phenomenon alleviates sterile-inflammation-induced uterine fibrosis in a mouse model of AS. Our liposome-mediated small RNA delivery is a novel therapeutic approach to alleviate pathological phenotypes of the endometrium with AS by modulating macrophage polarity *in vivo*. Finally, our results propose that miR-10a/MT-Lip could be used as a therapeutic platform to treat various inflammatory disorders by targeting macrophage polarization while maintaining enhanced patient safety.

RESULTS

Preparation and characterization of miRNA-encapsulated macrophage-targeting liposomes (miR/MT-Lips)

As illustrated in Figure 1A, we prepared liposomes through the conventional thin-film hydration method by adding various amounts of phospholipid and cholesterol to control liposome size.[31,32] The liposome size increased as the proportion of cholesterol in the total lipid increased (Figure 1B). The liposomes with larger particle sizes showed higher macrophage-specific internalization rates (Figures 1C and S1). A cationic polymer polyethyleneimine (PEI) was also employed to increase the encapsulation efficiency of miRNAs in the liposomes. Electrostatic complexes formed between cationic PEI and anionic miRNAs can improve interaction with anionic lipids. To find the optimal conditions for encapsulating PEI/miRNA in MT-Lip, we performed a gel retardation assay after forming PEI and miRNA complexes with various Nucleus/PEI (N/P) ratios. Electrostatic complexes of PEI-miR-10a were successfully formed at N/P ratios of 5, 10, and 20 (Figure S2A). Cell viability was approximately 60% at a PEI-miR-10a N/P ratio of 5, and cell viability tended to decline as the N/P ratio increased (Figure S2B). Based on these results, PEI/miRNA was prepared at an N/P ratio of 5 and encapsulated in MT-Lip for further experiments. Scramble miR-FAM/MT-Lip was prepared with or without PEI and then characterized, to assess the encapsulation efficiency of scramble miR-FAM/MT-Lip (Figure S3A). In the PEI-scramble miR-FAM group, ∼69% of the feed miRNA was encapsulated, as opposed to only 3% in the case of encapsulation of native miRNA without PEI (Figure S3B). Additionally, we observed scramble miR-FAM/MT-Lip internalization (intense green fluorescence) in macrophages, mainly in the presence of PEI (Figure S3C). The zeta potentials of MT-Lip, native miR-10a, the PEI-miR-10a complex, and miR-10a/MT-Lip were measured to be −26.8, −1.7, 31.7, and −5.2 mV, respectively (Figure 1D). These results indicate that the positively charged PEI-miR-10a complex was successfully encapsulated in the negatively charged lipid membrane. The miRNA-encapsulated MT-Lip was observed as a spherical shape in the transmission electron microscopy (TEM) image with a size of ∼1.24 μm (Figures 1E and 1F). Before *in vitro* cell experiments, the cytotoxicity of MT-Lip was evaluated in RAW 264.7 cells. The MT-Lip and miR/MT-Lip with or without PEI exhibited no toxicity (Figure 1G). Furthermore, intravenous delivery of miR-10a/MT-Lip did not affect the immune system and cause systemic toxicity in general (Figure S4).

Cellular internalization of miR/MT-Lip in macrophages

To confirm the macrophage-specific targeting of miRNA-encapsulated MT-Lip, we treated miRNA labeled with an MT-Lip-encapsulating fluorescent molecule (i.e., FAM) with HEK293T cells or RAW 264.7 cells. The cellular internalization of the liposome was evaluated using a fluorescence microscope and flow cytometry (Figure 2). As shown in Figure 2A, green fluorescence was observed in RAW 264.7 cells, but not in HEK293T cells. The flow cytometry data also showed that MT-Lip was internalized in 43.63% of RAW 264.7 cells but in only 9.44% of HEK293T cells (Figures 2B and 2C). In contrast, the PEI-miRNA complex showed non-specific cellular internalization (Figure S5). In fact, the cellular internalization of the PEI-scramble miR-FAM complex was significantly greater in HEK293T cells than in RAW 264.7 cells. Interestingly, $CD45^{+}CD11b^{+}F4/80^{+}$ bone marrow-derived macrophages (BMDMs) efficiently internalized MT-Lip with a significantly higher efficiency (95.96%) than RAW 264.7 cells (Figure S6).

To decipher the internalization mechanism(s) of MT-Lip in macrophages, we evaluated the internalization rates of MT-Lip after treating several inhibitors of internalization processes in RAW 264.7 cells 8(Figures 2D and 2E). Clathrin-dependent endocytosis inhibitors chlorpromazine (CPZ) and dynasore did not disturb its internalization, nor did the caveolar-dependent endocytosis inhibitor MβCD.[34] However, amiloride, a macropinocytosis inhibitor, and cytochalasin D (CytoD), an inhibitor for both phagocytosis and macropinocytosis,

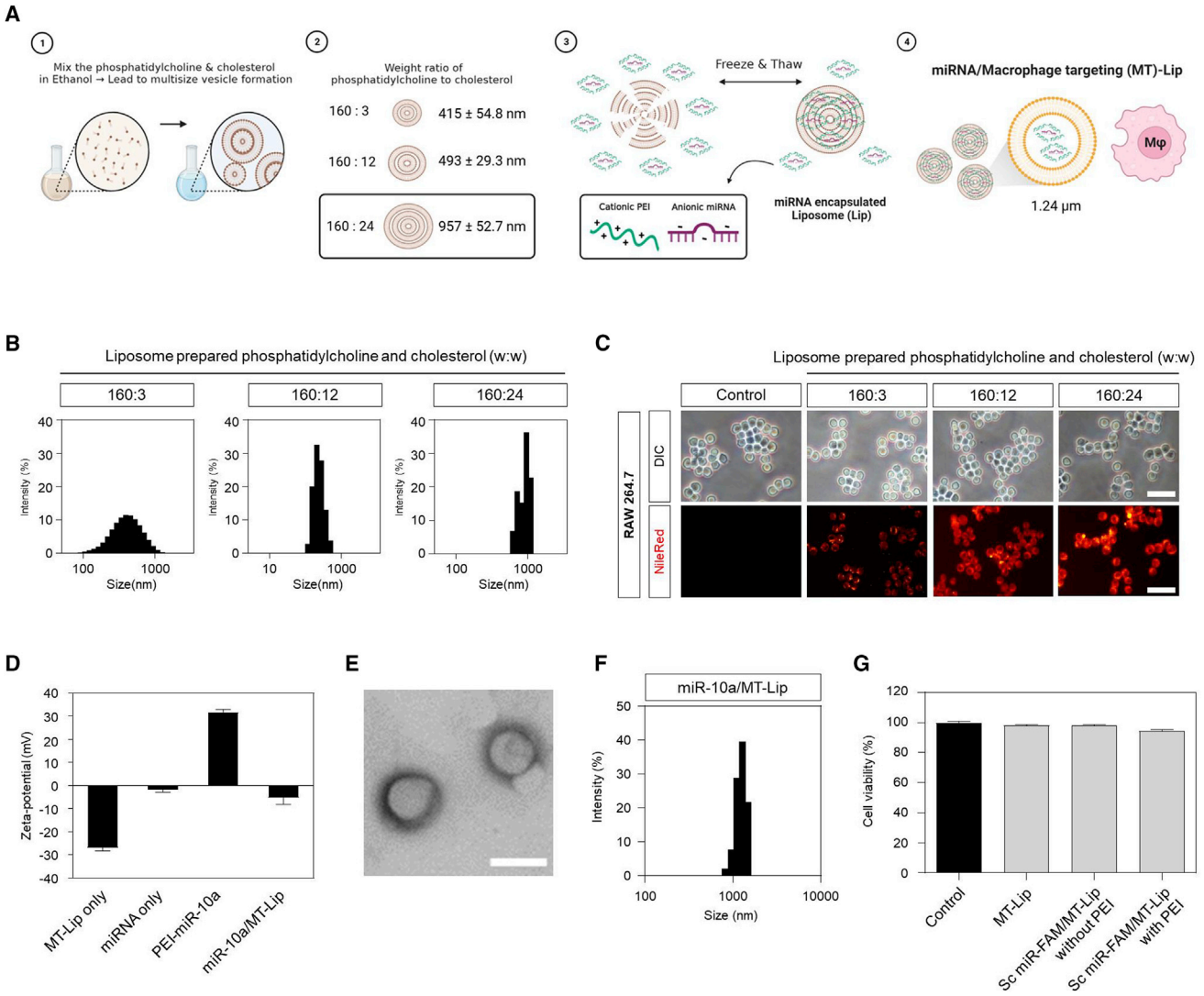

Figure 1. Preparation and characterization of liposome with controlled particle size to specifically target macrophage (MT-Lips)

(A) Schematic illustration of the MT-Lip preparation process: liposomes were prepared by thin-film hydration technique. The size of the liposome can be controlled by adjusting the weight ratio of phosphatidylcholine to cholesterol. A complex of cationic polyethyleneimine (PEI) and anionic miRNA is encapsulated in liposomes using the freeze and thaw process. Finally, MT-Lip with a size of approximately 1 μm was produced for macrophage targeting. Figure was created with BioRender.com. (B) Size distribution of liposomes prepared with various concentrations of cholesterol. (C) The fluorescent images of RAW 264.7 cells treated with size-controlled MT-Lip stained with NileRed. The scale bar represents 50 μm. (D) Zeta potentials of MT-Lip, miRNA miR-10a, the PEI-miR-10a complex (PEI-miR-10a), and miR-10a-encapsulated MT-Lips (miR-10a/MT-Lips). (E) Transmission electron microscopy (TEM) image of miR-10a/MT-Lip. The scale bar represents 1 μm. (F) Size distribution of miR-10a/MT-Lip. (G) Cell viability was quantified for RAW 264.7 cells treated with MT-Lip samples prepared under various conditions.

dramatically reduced MT-Lip cellular internalization, suggesting that the MT-Lip enters macrophages by macropinocytosis and possibly phagocytosis. The internalization of MT-Lip into macrophages was monitored over time using confocal microscopy (Figure 2F). We followed the intracellular distribution of MT-Lip carrying FAM-labeled scramble miRNAs (scramble miR-FAM, green). Cellular internalization of MT-Lip resulted in the accumulation of MT-Lip in endosomes (yellow in Figure 2F) labeled with LAMP1 (red). Only endosomes were visible until 1 h after liposome treatment; MT-Lip was detected in endosomes 2–4 h later. At 6 h, the scramble miR-FAM/MT-Lip signals exited endosomes and were released into the cytoplasm. These findings show that MT-Lip encapsulated with miRNAs is internalized via phagocytosis and/or macropinocytosis, and that delivered miRNAs then escape from the endosome in macrophages.

Control of macrophage polarization by miR-10a/MT-Lip

Next, the M2 polarization of macrophages by MT-Lip encapsulated with miR-10a (miR-10a/MT-Lip) was evaluated (Figure 3).

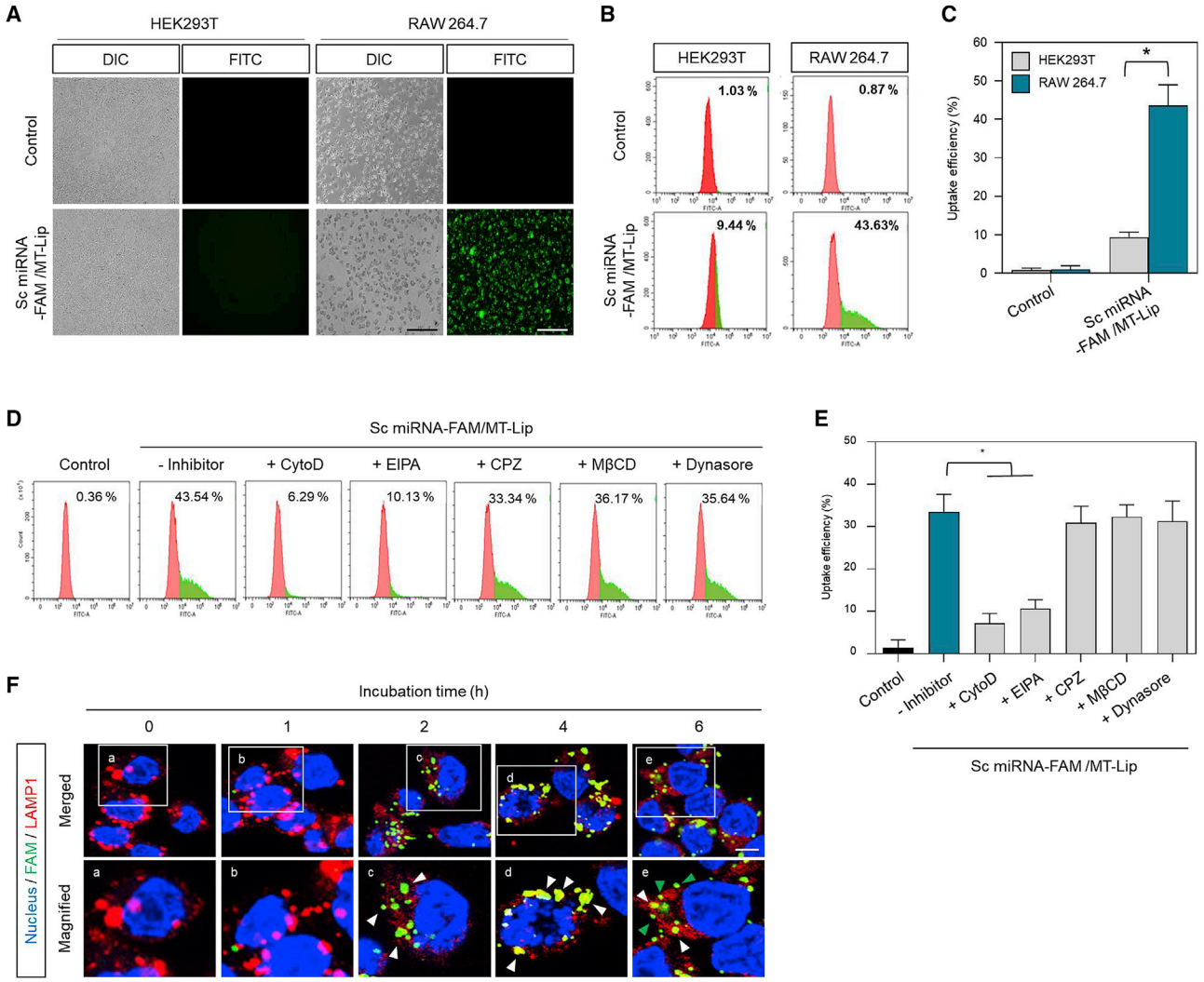

Figure 2. Evaluation of cellular internalization efficiency and cellular internalization mechanisms of MT-Lips

(A) Fluorescent images for evaluation of cellular internalization of scramble miR-FAM/MT-Lip in HEK293T and RAW 264.7 cells. The scale bar represents 150 μm. (B) Flow cytometry histograms for evaluation of cellular internalization of scramble miR-FAM/MT-Lip in HEK293T and RAW 264.7 cells. (C) Quantitative analysis of cellular internalization of scramble miR-FAM/MT-Lips in HEK293T and RAW 264.7 cells. Data are based on flow cytometry results. Each bar represents the mean ± standard deviation of three independent experiments. *$p < 0.05$. (D) Flow cytometry histograms to evaluate the internalization of scramble miR-FAM/MT-Lips in the presence of various internalization inhibitors in RAW 264.7 cells. (E) Quantitative analysis of cellular internalization of scramble miR-FAM/MT-Lips in the presence of various internalization inhibitors in RAW 264.7 cells. Data are based on the flow cytometry results. Each bar represents the mean ± standard deviation of three independent experiments. *$p < 0.05$. (F) Confocal microscopy images for evaluation of the process of cellular internalization of scramble miR-FAM/MT-Lip in RAW 264.7 cells. Confocal images show immunofluorescence staining for LAMP-1 (late endosome marker). Each bottom panel shows an enlarged image representing the white boxed area in the panel above. White arrowheads indicate the co-localization of scramble miR-FAM/MT-Lips and endosomes. Green arrowheads indicate scramble miR-FAM/MT-Lips escape from endosomes. The nucleus, FAM-labeled RNA, and endosome are represented in blue, green, and red, respectively.

miR-10a causes macrophage M2 polarization and is currently being investigated for the treatment of a variety of inflammatory disorders.[35,36] LPS is known to induce inflammatory responses by stimulating the Toll-like receptor 4 (TLR4) of monocytes and macrophages.[37] As seen in Figure 3A, we examined miR-10a/MT-Lip for the M2 polarization of macrophages *in vitro*. The expression profiles of M1- and M2-related markers were examined at the mRNA level after miR-10a/MT-Lip treatment in LPS-induced M1 macrophages. M1 markers remarkably increased in macrophages following LPS treatment, whereas M2 markers decreased. IL-4, an anti-inflammatory cytokine, was used as a control to induce M2 polarization in macrophages.[37,38] Similar to IL-4, miR-10a/MT-Lip decreased the expression of M1 markers *iNos* and *Socs3* and increased the expression of M2 markers *Arg1* and *Mrc1* (Figures 3B and 3C). Western blotting analyses demonstrated that miR-10a/MT-Lip treatment significantly decreased the expression of M1 markers (p-p65, p65, and inducible

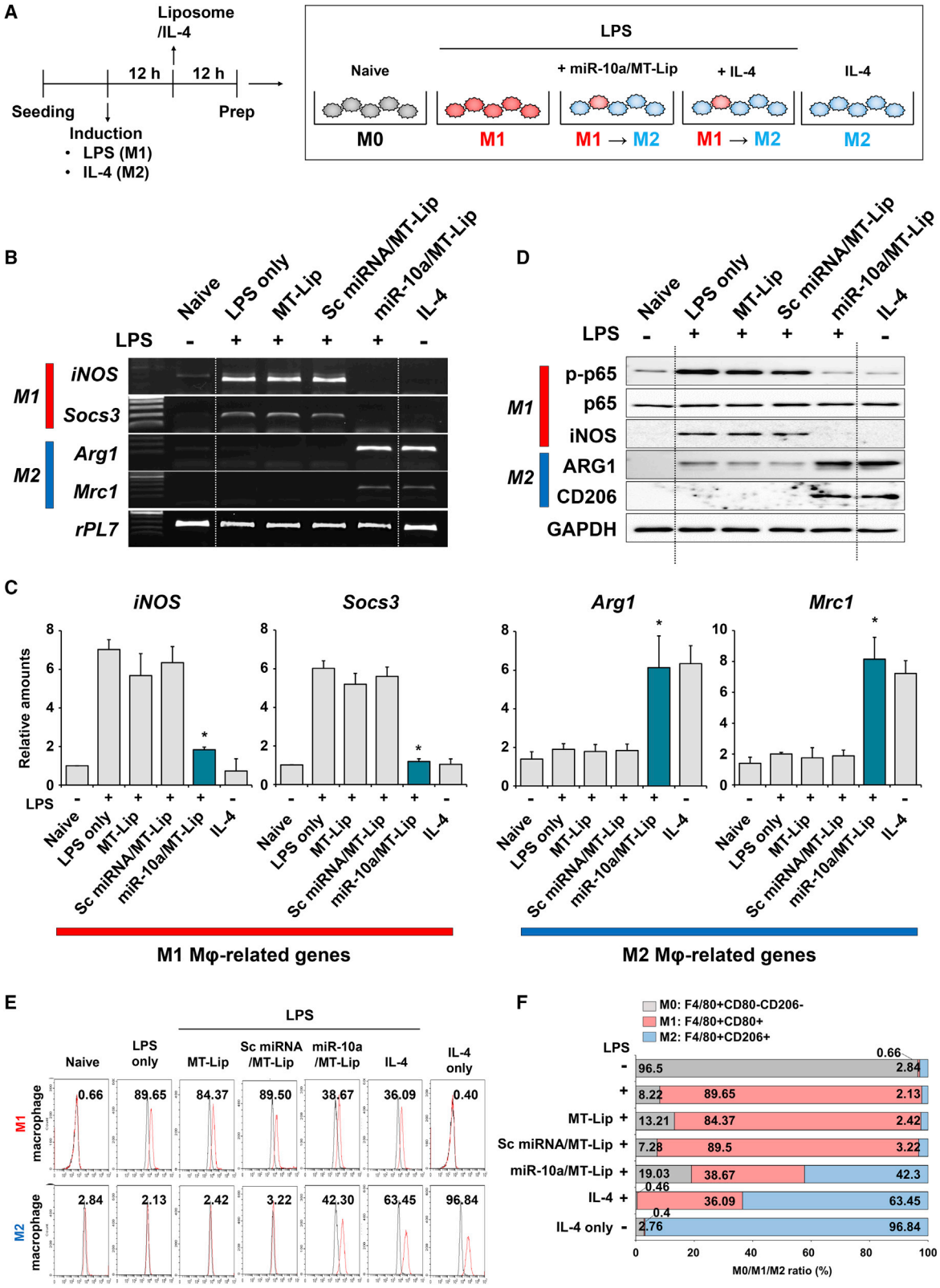

(legend on next page)

nitric oxide synthase [iNOS]) in macrophages while increasing the M2 markers (ARG1 and CD206), in agreement with the results at the mRNA level (Figure 3D). Interestingly, 38.67% and 36.09% of RAW264.7 cells treated with miR-10a/MT-Lip and IL-4 after the LPS challenge remained in the M1 population, respectively (Figures 3E and 3F), although miR-10a/MT-Lip and IL-4 significantly suppressed expression of M1 markers.

Macrophage-specific targeting of miR/MT-Lip to convert macrophage polarization *in vivo*

We then examined the *in vivo* functionality of miR-10a/MT-Lip for the M2 polarization of macrophages in mice conditioned with LPS for inflammation (Figure 4). As shown in Figure 4A, mice were treated with LPS to promote inflammation, followed by miR-10a/MT-Lip given intravenously 12 and 24 h later. miR-10a/MT-Lip doubled the proportion of M2-polarized macrophages without changing the number of M1 macrophages in the spleen of LPS-injected mice (Figure 4B). Although MT-Lip and scramble miRNA/MT-Lip did not affect the macrophage polarity in $CD45^+F4/80^+$ splenic macrophages, miR-10a/MT-Lip effectively decreased the M1/M2 ratio by increasing M2 macrophages from 12.8% to 25.9% (Figure 4C). miR-10a/MT-Lip did not alter the population of other immune cells, such as neutrophils, NK cells, T cells, B cells, or dendritic cells (DCs), in the spleen (Figure 4D). To evaluate macrophage-specific targeting of our miR/MT-Lip *in vivo* among immune cells, we analyzed splenocytes and peripheral blood mononuclear cells (PBMCs) after scramble miR-FAM/MT-Lip injection. Flow cytometry analysis revealed that the fluorescence signal of scramble miR-FAM was immediately observed (1 h after injection), mainly in splenic macrophages, and this signal became decreased with time (Figure 4E). However, this signal was barely detected in splenic neutrophils, NK cells, T cells, B cells, DCs (Figure 4E), and PBMCs (Figure 4F). These results collectively suggest that miR-10a/MT-Lip specifically targets macrophages without disturbing other immune cells in the mouse spleen with inflammation induced by LPS.

Evaluation of therapeutic efficacy of miR-10a/MT-Lip in a mouse model of AS

Finally, we evaluated the therapeutic effects of miR-10a/MT-Lip in targeting macrophages to modulate their polarity in a mouse model of AS characteristic of sterile inflammation and fibrosis.[39] AS was induced in the uterus by physical insults as described in our previous study,[39] and miR-10a/MT-Lip was administered intravenously 2, 4, and 7 days afterward (Figure 5A). miR-10a/MT-Lip treatment effectively decreased the M1/M2 ratio by increasing the M2 macrophage population from 28.75% to 35.37% at 3 days after miR-10a/MT-Lip treatment (Figure 5B). To examine macrophage-specific targeting of miR/MT-Lip in the damaged uterus with AS, major uterine cells, including immune cells, were prepared and analyzed 1 and 6 h after the third delivery of scramble miR-FAM/MT-Lip. Flow cytometry analyses of uterine cells showed that the fluorescence signal of scramble miR-FAM at 1 h after delivery was mainly detected in uterine macrophages, but not in uterine epithelial and stromal cells and other immune cells (Figure 5C). The intensity of scramble miR-FAM/MT-Lip further accumulated in uterine macrophages, but not any other cell types, at 6 h after delivery.

miR-10a/MT-Lip treatment significantly reduced the expression of M1 markers *iNos* and *Socs3* while increasing the expression of M2 markers *Arg1* and *Mrc1* in the uterus with AS (Figure 5D). Hydroxyproline assay showed that miR-10a/MT-Lip significantly reduced collagen deposition, a representative feature of fibrosis, in the uterus with AS (Figure 5E). Real-time reverse transcription PCR (RT-PCR) analyses showed that miR-10a/MT-Lip therapy dramatically reduced the expression of fibrosis-associated genes (Figure 5F) and increased the expression of angiogenesis-related genes (Figure 5G) in the uterus with AS. Immunofluorescence staining for collagen 1A1 (COL1A1), a well-known fibrosis marker, clearly supported the notion that miR-10a/MT-Lip therapy significantly reduces fibrosis in the damaged uteri of mice with AS (Figure 5H). Furthermore, immunofluorescence staining for CD31, an endothelial cell marker, and KI-67, a cell proliferation marker, demonstrated that miR-10a/MT-Lip therapy significantly increased angiogenesis in the damaged uterus with AS (Figures 5H and 5I). These findings collectively suggest that miR-10a/MT-Lip therapy successfully restored the imbalanced M1/M2 ratio in the uteri of mice with AS, alleviating chronic inflammation followed by fibrosis.

DISCUSSION

Macrophages found in various tissues become polarized in response to changes in their environment, resulting in the formation of distinct macrophage subtypes such as M1 and M2 macrophages.[13] In particular, it is critical to enhance macrophage polarization to M2 to treat inflammatory disorders.[40,41] M2 polarization inducers must be specifically delivered to macrophages to efficiently generate M2 polarization of macrophages *in vivo*. Effective delivery of drugs to macrophages has already been accomplished by using active targets with targeting ligands or passive targets with particle size control.[42–44] Although an active targeting technique based on targeting ligands such as antibodies or mannose has been developed,[45–47] a conjugation process between the targeting ligand and the particle is necessary, as is purification. The strategy of targeting macrophages via particle size

Figure 3. M2 polarization of macrophages induced by miR-10a/MT-Lips

(A) Schematic illustration of *in vitro* experiment. (B) Changes in M1-and M2-related mRNA expression associated with miR-10a/MT-Lip treatment in RAW 264.7 cells analyzed by reverse transcription PCR (RT-PCR). (C) Changes in M1- and M2-related mRNA expression associated with miR-10a/MT-Lip treatment in RAW 264.7 cells analyzed by real-time RT-PCR. Each bar represents the mean ± standard deviation of three independent experiments. *$p < 0.05$. (D) Changes in M1- and M2-related protein expression associated with miR-10a/MT-Lip treatment in RAW 264.7 cells analyzed by western blotting. (E) Flow cytometry histogram for evaluating the population of M0, M1, and M2 macrophages. Macrophages were labeled with M0 ($F4/80^+CD80^-CD206^-$), M1 ($F4/80^+CD80^+$), and M2 ($F4/80^+CD206^+$) markers for flow cytometry analysis. (F) Bar graph of flow cytometry data from (E), i.e., proportions of macrophages polarized to M1 or M2 after miR-10a/MT-Lip treatment.

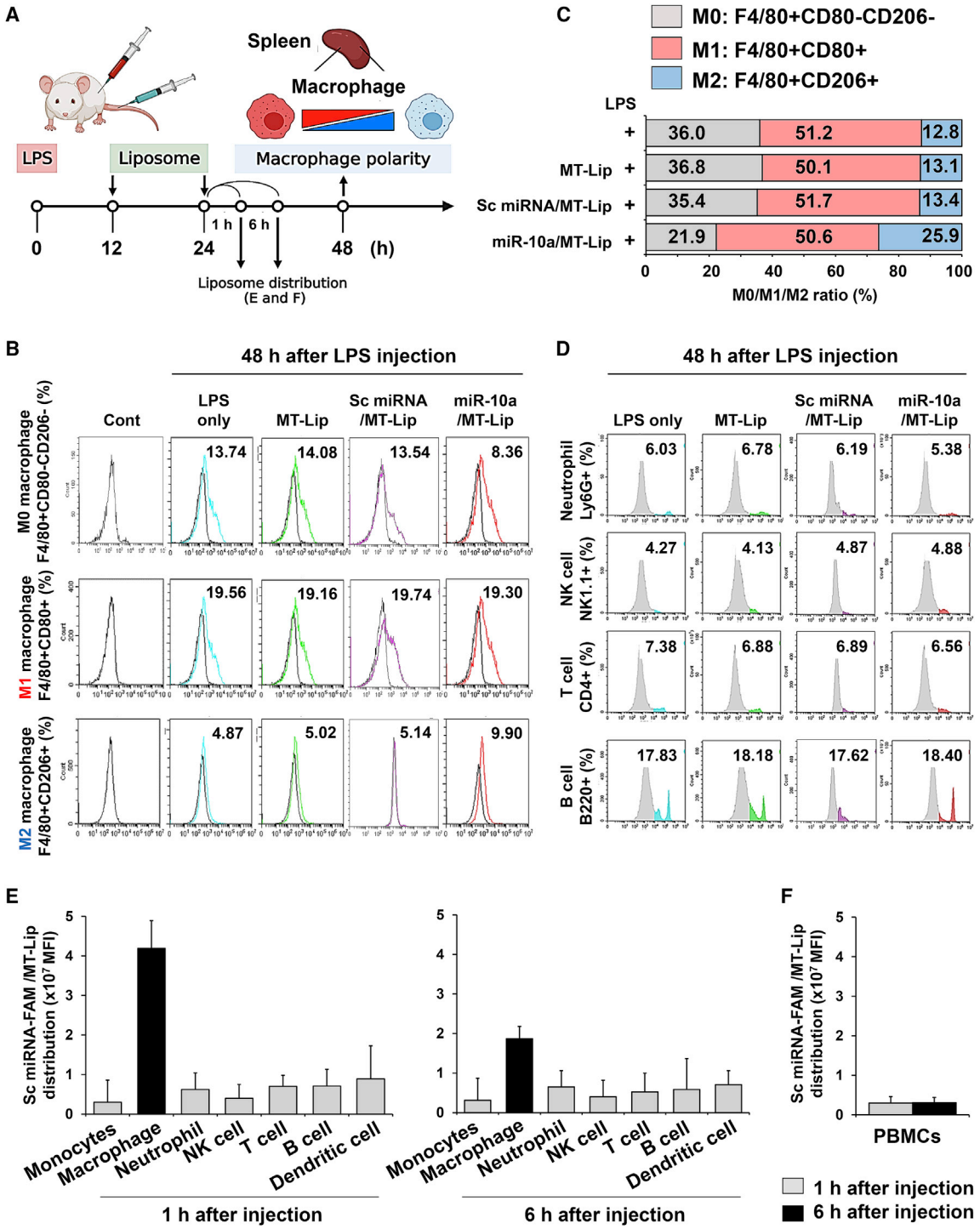

Figure 4. M2 polarization of macrophages by miR-10a/MT-Lips *in vivo*

(A) Schematic illustration of *in vivo* experiment. Figure was created with BioRender.com. (B) Flow cytometry histogram for population evaluation of M0, M1, and M2 macrophages *in vivo*. Macrophages were isolated from the spleen and labeled with M0 ($F4/80^+CD80^-CD206^-$), M1 ($F4/80^+CD80^+$), and M2 ($F4/80^+CD206^+$) markers for flow cytometry analysis. (C) Bar graph of flow cytometry data from (B), i.e., proportions of macrophages polarized to M1 or M2 *in vivo* after miR-10a/MT-Lip treatment. (D) Flow cytometry histograms evaluate changes in populations of various immune cell types associated with miR-10a/MT-Lip treatment *in vivo*. (E and F) Flow cytometry analysis of scramble miR-FAM/MT-Lip distribution following intravenous delivery in mice. Immune cells in the spleen (E) and peripheral blood mononuclear cells (F) were analyzed 1 and 6 h after intravenous delivery of scramble miR-FAM/MT-Lips. The mean fluorescent intensity of scramble miR-FAM in each immune cell population is shown in the graph.

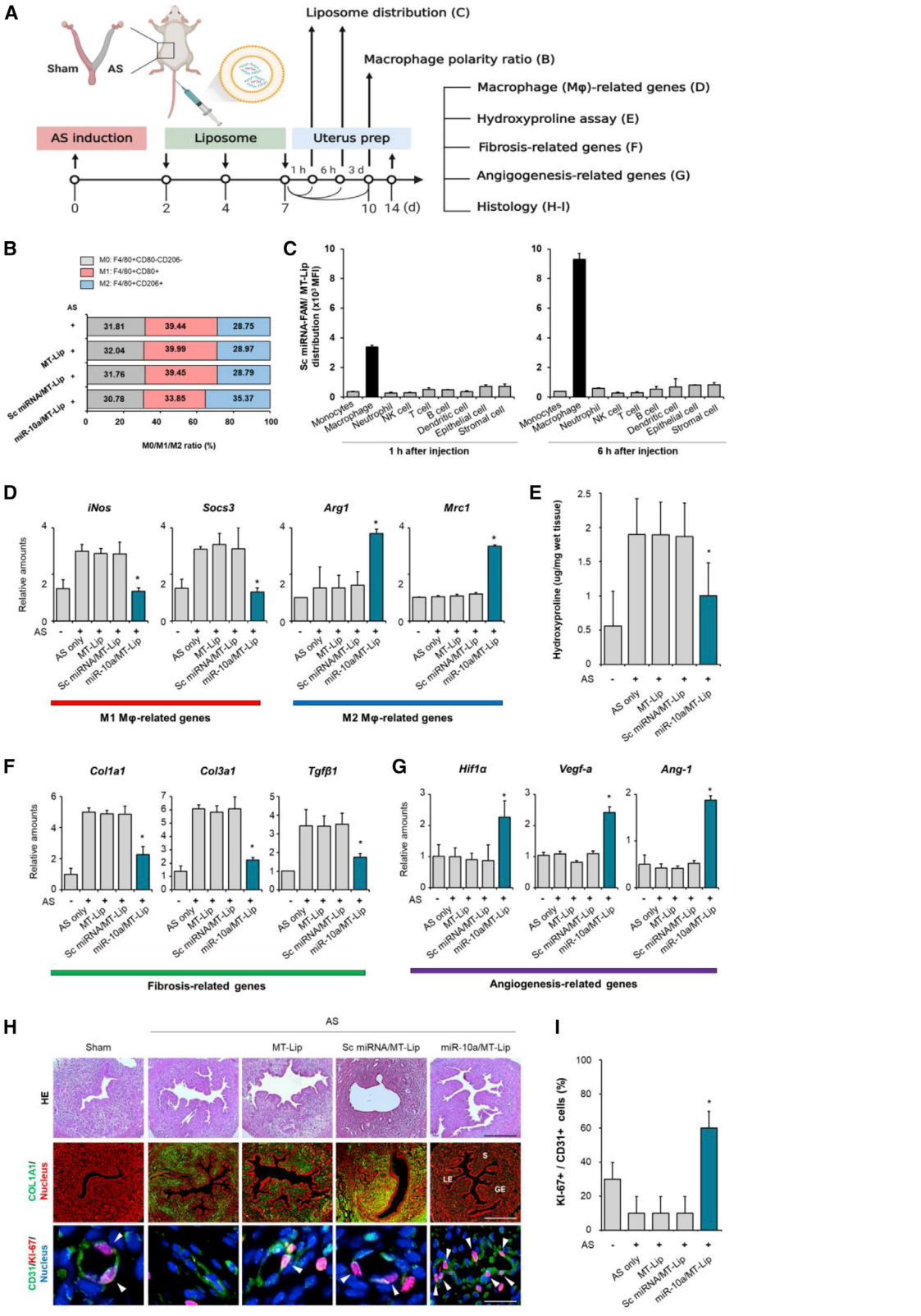

(legend on next page)

control has the process advantage of reasonably straightforward production. It is well established that macrophages identify and phagocytose particles larger than 500 nm in size.[29,30] By carefully regulating the cholesterol level throughout the liposome synthesis process, we were able to successfully construct MT-Lip with a diameter of approximately 1 μm; this size-delimited MT-Lip was well internalized by macrophages.

This study employed miR-10a, which is known to induce macrophage M2 polarization.[35] Previous investigations have shown that miR-10a blocks the pro-inflammatory nuclear factor κB (NF-κB) pathway.[48–50] However, naked miRNA has limitations: poor stability *in vivo* and difficulty in specifying delivery solely to macrophages. Internalization of miR-10a into macrophages was promoted in this study using liposomes with controlled particle size. The cholesterol ratio was tuned to control the particle size of the liposome. As illustrated in Figure 1A, the particle size increased dependent on the cholesterol content. PEI, a cationic polymer, was employed to efficiently encapsulate miR-10a in MT-Lip. Cationic PEI created an electrostatic combination with anionic miR-10a, enhancing the encapsulation efficacy (Figure S1). Although the PEI-miR-10a complex was cytotoxic when unencapsulated (Figure S1), it was non-toxic when encapsulated in MT-Lip (Figure 1G). The cytotoxicity of PEI-miR-10a is thought to be due to cell membrane damage caused by the cationic-charged polyplex.[51–53] However, effective toxicity is reduced by the anionic lipid's masking of the positive charge of the PEI/miRNA encapsulated in the liposome, implying the biocompatibility of MT-Lip and miRNA/MT-Lip. As shown in Figure 2, scramble miR-FAM/MT-Lip particles were internalized by macrophages via phagocytosis or macropinocytosis, presumably because of scramble miR-FAM/MT-Lip's relatively large size of ∼1 μm.[29,30]

Our miR-10a/MT-Lip particles systemically reduced the M1/M2 ratio of splenic macrophages without provoking other immune cells *in vivo* (Figure 4). Furthermore, miR-10a/MT-Lip efficiently repolarized LPS-driven M1 phenotypes in macrophages *in vitro* at a level comparable with the key anti-inflammatory cytokine IL-4 (Figure 3). This finding suggests the macrophage specificity of MT-Lip. However, DCs differentiated from monocytes encounter phagocytosed antigens or pathogen-like macrophages in peripheral tissues.[54] Considering the similar phagocytic activities between macrophages and DCs, it is important to mention that DCs in the spleen after the LPS challenge (Figure 4E) and in the uterus with AS (Figure 5C) did not internalize scramble miR-FAM/MT-Lip as efficiently as macrophages. The functional difference between both immune cells in this study could be caused by two different functional states of DCs, immature and mature.[55] Immature DCs actively internalize antigens, but once immature DCs become mature under stimulation by inflammatory and pathogenic signals, they decrease phagocytic capacity and upregulate expression of MHC class II.[56] Because the spleen (in Figure 4) and uterus (in Figure 5) were challenged by LPS and physical trauma, respectively, we assume that DCs in the spleen and uterus faced inflammatory signals from LPS and AS so that they became mature in these conditions. It is consistent with the result that immature DCs derived from bone marrow internalize scramble miR-FAM/MT-Lip as efficiently as RAW 264.7 cells (Figure S6). These data suggest that macrophage-specific targeting with various carriers, including liposomes and NPs, may constitute an effective strategy for treating diseases in preclinical animal models.[57] Taken together, this approach may significantly benefit patients suffering from inflammatory diseases in future clinical applications of this technology. However, the safety and delivery mechanisms of macrophage-specific carriers should be clearly evaluated before human clinical trials.

Proinflammatory M1 macrophages exacerbate the pro-fibrotic process in inflamed tissues.[58] In this circumstance, M1 macrophages activate myofibroblasts by releasing matrix metalloproteinases (MMPs) that promote epithelial/endothelial-to-mesenchymal transition (EMT) and fibroblast recruitment for fibrosis. In contrast, M2 macrophages contribute to an anti-inflammatory environment and promote the healing and regeneration of wounds.[59] In this point of view, M2 macrophages become a friend to support tissue-repair processes. However, when the insult is not properly controlled, M2 macrophages could act as an enemy for tissue homeostasis. Excessive M2 macrophage in the M1/M2 ratio promotes a pro-fibrotic environment by producing a large amount of pro-fibrotic factors, such as transforming growth factor β (TGF-β), that promote myofibroblast proliferation, EMT activation, and collagen deposition.[60,61] M2 represents a breakpoint between wound healing and aggravation of the profibrotic process depending on microenvironments.[62] Whereas a persistent inflammatory environment pushed the M1/M2 ratio to an M1-biased condition in the uterus with AS (Figure 5), excessive profibrotic M2 macrophages (reduced M1/M2 ratio) caused fibrosis in mouse lung

Figure 5. Evaluation of therapeutic efficacy of miR-10a/MT-Lips in a mouse model of Asherman's syndrome (AS)

(A) Schematic illustration of *in vivo* therapeutic experiment using miR-10a/MT-Lips. Figure was created with BioRender.com. (B) Flow cytometry histogram for population evaluation of M0, M1, and M2 macrophages *in vivo*. Macrophages were isolated from the uterus and labeled with M0 ($F4/80^+CD80^-CD206^-$), M1 ($F4/80^+CD80^+$), and M2 ($F4/80^+CD206^+$) markers for flow cytometry analysis at 3 days after miR-10a/MT-Lip treatment. (C) Flow cytometry analysis of scramble miR-FAM/MT-Lip distribution following intravenous delivery in mice. Immune and uterine cells were analyzed 1 and 6 h after intravenous delivery of scramble miR-FAM/MT-Lips. The mean fluorescent intensity of scramble miR-FAM in each immune cell population is shown in the graph. (D) Changes in M1 and M2 polarization-related mRNA expression *in vivo* associated with miR-10a/MT-Lip treatment as analyzed by real-time RT-PCR. *iNos* and *Socs3* are involved in macrophage M1 polarization, while *Arg1* and *Mrc1* have been involved in macrophage M2 polarization. (E) Hydroxyproline content after miR-10a/MT-Lip treatment in uteri with AS. (F) Real-time RT-PCR analyses measuring miR-10a/MT-Lip treatment-associated changes in expression of fibrosis-related mRNAs in the uterus with AS. *Col1a1*, *Col3a1*, and *Tgfβ1* are well-known fibrosis-related genes. (G) Real-time RT-PCR of angiogenesis-related genes, such as *Hif1α*, *Vegf-a*, and *Ang-1*, after miR-10a/MT-Lip treatment. Each bar represents the mean ± standard deviation of three independent experiments. *$p < 0.05$. (H) Histological changes in the endometrium associated with miR-10a/MT-Lip treatment in uteri with AS. Histological analysis was performed by hematoxylin and eosin (H&E) staining and COL1A1, CD31, and KI-67 immunofluorescence staining. White arrowheads indicate proliferating endothelial cells (red nuclei). (I) Quantification of results in (H). GE, glandular epithelium; LE, luminal epithelium; S, stroma.

treated with bleomycin where M2-to-M1 conversion is required to mitigate fibrosis.[63,64] Therefore, M1 macrophage-directed regulation of inflammation and timely polarization toward regenerative M2 macrophages are essential to accomplish successful tissue repair.

Macrophages could be a key player in uterine regeneration under physiological and pathological conditions. Macrophages are likely to play a key role during menstruation, which requires tissue clearance and regeneration for the next cycle. These processes reach their peak at 6%–15% of all cells within the endometrium during the menstrual period following progesterone withdrawal.[65] In the endometrium of patients with AS, not only the total macrophage count but also the M2 macrophage count significantly decreased in the endometria of patients with AS, possibly because of the down-regulation of Colony stimulating factor 1 (CSF1), which is critical for macrophage differentiation.[66] Furthermore, the M2 macrophage secretome promotes the proliferation and migration of endometrial epithelial cells *in vitro*, suggesting the possibility of macrophage modulation as a therapeutic option for AS. In mice with AS, miR-10a/MT-Lip treatment not only considerably elevated the expression of M2 markers (Figure 5D) but also significantly reduced the expression of fibrosis-related genes and fibrotic regions in the uterus (Figures 5E, 5F, and 5H). It is believed that miR-10a/MT-Lip facilitates the M1-to-M2 polarization conversion of macrophages, alleviating sterile inflammation and thus reducing uterine fibrosis. M2 macrophage transfer regulates the TGF-β/Smad7 pathway to reduce renal injury, viral myocarditis, and acute nephritis. These connections indicate that M2 macrophages have a protective role in tissue recovery, and that M2 macrophage transplantation can serve as potential cell therapy in disease treatment.[67] Thus, M2 macrophages repolarized by miR-10a/Lip treatment in this study may have therapeutic potential in recovery from uterine fibrosis. Although a miRNA was used in this work to modulate macrophage polarization, our treatment concept could be extended in the future by using mRNA-based therapeutics. Additionally, by developing the scope of knowledge gained in this work to include various polymers or inorganic nanoparticles, as well as lipid nanoparticles, it may be possible to use this platform in the targeted treatment and imaging of macrophages. This platform technology is likely to be used to treat various inflammatory illnesses in the future, including IBD. The MT-Lip technology developed in this study is expandable to macrophage-targeting drug-delivery platforms encapsulated with miRNA and other nucleic acid therapeutics and chemical drugs.

MATERIALS AND METHODS

Materials

All reagents and solvents were obtained commercially and used without further purification. Phosphatidylcholine, cholesterol, ethanol, PEI (branched, 25 kDa), NileRed, CytoD, amiloride hydrochloride hydrate (amiloride), CPZ, MβCD, dynasore hydrate (dynasore), Tween 20, and Triton X-100 were purchased from Sigma-Aldrich (St. Louis, MO, USA). Chloroform was purchased from Daejung (Siheung, Republic of Korea). Fluorescein-labeled negative control miRNA (scramble miR-FAM, Negative control) and 10a mimic miRNA (miR-10a, 5′-UACCCUGUAGAUCCGAAUUUGUG-3′) were purchased from BIONEER (Daejeon, Republic of Korea). Dulbecco's modified Eagle's medium (DMEM), antibiotics (penicillin/streptomycin), Dulbecco's phosphate-buffered saline (PBS; DPBS), and trypsin-EDTA solution (trypsin, 1X) were obtained from Hyclone (Logan, UT, USA). PBS (1X, pH 7.4) and fetal bovine serum (FBS) were obtained from Gibco BRL (Invitrogen, Carlsbad, CA, USA). A D-Plus CCK cell viability assay kit (CCK-8) was purchased from Donginbiotech (Seoul, Republic of Korea). Protein block serum was purchased from Dako (Carpinteria, CA, USA). BSA and DAPI were obtained from Thermo (Rockford, IL, USA). 4% paraformaldehyde (PFA) was obtained from BioPrince (Gangwon, Republic of Korea). TRIzol reagent was obtained from Ambion (Carlsbad, CA, USA). Moloney Murine Leukemia Virus (M-MLV) reverse transcriptase was obtained from Promega (Madison, WI, USA). SYBR Green Dye, TBS, skimmed milk powder, nitrocellulose membrane, and an enhanced chemiluminescence (ECL) western blotting substrate kit were obtained from Bio-Rad (Waltham, MA, USA). PRO-PREP was obtained from iNtRON (Seongnam, Republic of Korea). A phosphatase inhibitor was purchased from Roche Applied Science (Indianapolis, IN, USA).

Preparation of MT-Lip

In a round-bottom flask, phosphatidylcholine 710 μL (1 mg/mL in ethanol) and cholesterol were mixed at various weight ratios (160:3, 160:12, and 160:24) in ethanol (2 mL). After dispersion, the solvent was completely removed using a vacuum rotary evaporator, forming a thin, uniform translucent film on the flask walls. PBS (2 mL) was added to the flask to dissolve the film. The liposomal suspension was sonicated in a water bath for 6 min and hydrated using a rotary evaporator for 2 h. Liposomes were pelleted by centrifuging at 4°C and 8,000 rpm for 20 min. The supernatant was decanted, and the liposomes were redispersed in PBS (2 mL). This process was repeated twice, finally yielding MT-Lip.

Gel retardation assay

Electrophoresis was used to determine the ability of miRNA and PEI to form electrostatic complexes. PEI-miRNA complexes produced at various N/P ratios were mixed with 6× loading buffer and electrophoresed on a 1% agarose gel. Chemi-doc was used to photograph the gel (Chemi Doc MP System; Bio-Rad, Hercules, CA, USA).

In vitro cytotoxicity test

Cells were seeded at 2.5×10^5 cells/well to evaluate cytotoxicity in 12-well plates. PEI-miRNA complexes (mass of RNA: 1 μg) were incubated with cells for 4 h at various N/P ratios. Cells were then rinsed with DPBS and incubated for 2 h at 37°C in serum-free media containing 10% CCK-8 solution (Dojindo, Tokyo, Japan). The absorbance at 450 nm was determined using a microplate reader (Synergy H1 Microplate Reader; BioTek).

Preparation of miR/MT-Lip

For miRNA encapsulation in MT-Lip, a complex of PEI and miRNA (PEI-miRNA) was prepared as follows. miRNA and solutions of PEI in distilled water were mixed gently by pipetting at room temperature, resulting in various N/P ratios (0, 0.1, 0.5, 1, 5, 10,

and 20). PEI-miRNA was added to MT-Lip to achieve final miRNA and lipid weights of 1 mg and 2 μg, respectively. After five rapid freeze-thaw cycles, the mixture was pelleted by centrifuging at 4°C and 8,000 rpm for 35 min. The supernatant was decanted, and liposomes were redispersed in PBS (100 μL). The centrifugation and decantation processes were repeated once. Finally, miRNA/MT-Lip (120 pmol miRNA/MT-Lip) was stored at 4°C for subsequent use.

Evaluation of immune cell profiles and general toxicity after intravenous delivery of miR/MT-Lip

Whole blood was withdrawn 24 h after intravenous delivery of saline or miR-10a/MT-Lip into mice. As described previously, immune cell profiles and general toxicity were immediately evaluated in these blood samples.[39]

Measurement of miRNA encapsulation efficiency in MT-Lip

The fluorescence intensity of encapsulated scramble miR-FAM in scramble miR-FAM/MT-Lip was evaluated using a microplate reader set to excitation = 500 nm and emission = 560 nm. The encapsulation efficiency of miRNA in MT-Lip was calculated based on the measured fluorescence intensity.

Characterization of MT-Lip

MT-Lip particle size distribution and zeta potential were determined by Dynamic Light Scattering (DLS) (Zetasizer Nano ZS; Malvern Instruments, Malvern City, UK). MT-Lip particle size was measured using a disposable plastic cuvette with an equilibration time of 1 min. After completion of the size measurement, the zeta potential was measured using a zeta cuvette with an equilibration time of 1 min. The morphology of miR-10a/MT-Lip was observed by scanning electron microscopy (SEM; Hitachi, Chiyoda, Tokyo, Japan) and transmission electron microscopy (TEM; H-7600, Hitachi). For TEM observation, negative staining was performed with a 2% uranyl acetate solution.

Cell culture

Cell lines (human embryonic kidney cells, HEK293T; murine macrophage cells, RAW 264.7) were used for experiments. Cells were maintained with culture media made of DMEM (Hyclone) containing 10% FBS (Gibco) or 1% penicillin/streptomycin (DMEM; Hyclone) incubated at 37°C under a 5% CO_2 atmosphere. The DC2.4 cells, mouse DC line, were cultured in RPMI 1640 medium supplemented with 10% FBS (Gibco) and 1% penicillin/streptomycin (Hyclone) incubated at 37°C under a 5% CO_2 atmosphere.[68]

Isolation of bone marrow cells

Bone marrow cells were isolated from tibias and femurs of C57BL/6 male mice. Cells were collected in a 5-mL round-bottom tube with a cell strainer cap (Falcon, San Jose, CA, USA) via flushing the bone marrow with DPBS added to 2% FBS (Gibco). Cells were centrifuged at 500 × *g*, washed with DPBS added to 2% FBS, and incubated with red blood cell (RBC) lysis solution (BioLegend, San Diego, CA, USA) for 5 min at 4°C. After being washed with DPBS added to 2% FBS, collected cells were seeded for 7 days with 25 ng/mL macrophage colony stimulating factor (M-CSF; PeproTech, Rocky Hill, NJ, USA) into RPMI medium (Gibco) supplemented with 10% FBS and 1% penicillin/streptomycin (DMEM; Hyclone) incubated at 37°C under a 5% CO_2 atmosphere. The attached cells are macrophages, and the supernatant cells are DCs. The rate of differentiation to macrophage was analyzed by staining CD45, CD11b, and F4/80, and DCs were analyzed by staining CD11c.[69]

Cellular uptake

Cells were seeded at 1×10^6 cells/well in six-well plates in culture media. To confirm uptake according to liposome size, MT-Lip samples were stained with NileRed. The MT-Lip or scramble miR-FAM/MT-Lip was treated with cells at a concentration of 2 mg/mL for 4 h. After treatment, cells were washed with DPBS (Hyclone) before a DMEM change. After 24 h, the cellular internalization of MT-Lip was visualized by fluorescence microscopy (ECLIPSE Ti2-A; Nikon).

Flow cytometry

For flow cytometry analysis on a Beckman Coulter Flow Cytometer with CyExpert software (Beckman Coulter, Brea, CA, USA), cells were detached with 0.25% trypsin and centrifuged at 500 × *g* for 5 min at 4°C. The supernatant was removed, and the cell pellet was resuspended with 0.1% BSA (Thermo) in 1× DPBS (Hyclone) three times. The data represent the mean fluorescent signals from 30,000 cells. Antibodies used for flow cytometry are shown in Table S1.

Inhibition of endocytosis

To inhibit the endocytosis pathway, we used five different pharmacological inhibitors: 20 μM CytoD (an inhibitor of phagocytosis; Sigma-Aldrich), 50 μM amiloride (an inhibitor of macropinocytosis; Sigma-Aldrich), 10 μM CPZ (an inhibitor for clathrin-coated vesicles; Sigma-Aldrich), 100 mM methyl-β-cyclodextrin (MβCD; an inhibitor for the formation of caveolin-coated vesicles; Sigma-Aldrich), and 50 μM dynasore (an inhibitor for the scission of clathrin- and caveolin-coated vesicles; Sigma-Aldrich). Each inhibitor was pretreated in RAW 264.7 for 1 h before incubation with liposomes for 4 h in the presence of inhibitors. After treatment, the cellular internalization of MT-Lip was measured by flow cytometry.

Immunofluorescence staining

RAW 264.7 was fixed in 4% PFA (BioPrince) for 15 min and permeabilized for 15 min in 0.2% Triton X-100 (Sigma-Aldrich) in PBS (Gibco). After three washings, non-specific staining was blocked using protein block serum for 1 h. Cells were then incubated with appropriate primary antibodies overnight at 4°C. The following day, cells were incubated with a secondary antibody for 1 h at room temperature. After three washings in PBS (Gibco), cells were counter-stained for nuclei with DAPI (1:1,000; Thermo) for 10 min and mounted. Images were obtained using a confocal microscope (Zeiss LSM880; Carl Zeiss, Oberkochen, Germany) and analyzed using the accompanying software (ZEN, Carl Zeiss). The detailed information for primary and secondary antibodies is summarized in Table S1.

RNA preparation, RT-PCR, and real-time RT-PCR

According to the manufacturer's protocols, total RNA was extracted from the RAW 264.7 using TRIzol reagent (Ambion). One microgram of total cellular RNA was subjected to RT using M-MLV (Promega) reverse transcriptase with random primers and oligo dT for cDNA synthesis. Synthesized cDNA was used for PCR with specific gene primers at appropriate cycle numbers and annealing temperatures (Table S2). The PCR products were subjected to electrophoresis. For quantification of expression levels, real-time RT-PCR was performed using SYBR Green Dye (Bio-Rad). A standard curve of cycle thresholds for several serial dilutions of a cDNA sample was established and used to calculate each gene's relative abundance to compare transcript levels among samples. Values were then normalized to the relative amounts of rPL7 cDNA. All PCRs were performed in duplicate.

Western blotting

RAW 264.7 was lysed in a lysis buffer of PRO-PREP (iNtRON) solution and 1× phosphatase inhibitor (Roche Applied Science). The protein samples (10–20 μg/lane) were then separated by 8%–15% SDS-PAGE, transferred onto a nitrocellulose membrane (Bio-Rad), and blocked with 5% skim milk (Bio-Rad) in TBS (Bio-Rad) containing 0.1% Tween 20 (Sigma-Aldrich). After blocking, membranes were subjected to western blotting with appropriate primary antibodies overnight at 4°C. The following day, membranes were incubated with a secondary antibody in 5% skim milk for 1 h at room temperature. The signals were developed using an ECL western blotting substrate kit (Bio-Rad) and detected using Chemi-doc XRS+ (Bio-Rad) with Image Lab 5.2 software (Bio-Rad). The detailed information for primary and secondary antibodies is summarized in Table S1.

Lipopolysaccharide (LPS)-induced *in vivo* inflammation model

According to institutional guidelines for laboratory animals, all mice used in this study were housed in the Animal Care Facility of CHA University. This study was approved by the Institutional Animal Care and Use Committee (approval number 200159). Eight-week-old C57BL/6 female mice were provided by Orient Bio (Gapyeong, Gyeonggi, Republic of Korea), housed under temperature- and light-controlled conditions for 12 h daily, and fed *ad libitum*. Mice received a single dose of LPS (5 mg/kg) by intraperitoneal injection. At 12 and 24 h after LPS administration, MT-Lip with or without miRNA was injected intravenously.

Isolation of splenic immune cells

The spleen was smashed and ground between the rough sides of frosted glass slides and then treated with 1 mL of an enzyme cocktail containing Collagenase D (Sigma-Aldrich), DNase I (Sigma-Aldrich), and Dispase (Gibco) in HBSS (Gibco) containing 2% FBS (Gibco). Cell suspensions were passed through a 100-μm nylon cell strainer (Invitrogen), followed by resuspension of the cells. For lysis of RBCs (BioLegend), cells were incubated with 1 mL of RBC lysis buffer (BioLegend) for 2 min, washed with washing buffer (with 0.1% BSA in 1× DPBS), and centrifuged at 500 × *g* for 5 min at 4°C. The supernatant was removed, and the cell pellet was resuspended with washing buffer three times. The cells were treated with fluorochrome-conjugated rat anti-mouse antibodies for 30 min at room temperature. Flow cytometry was used to examine cells after rinsing in washing buffer. Table S1 lists the antibodies used in flow cytometry.

Experimentally induced murine model of AS

As previously reported,[39] 8-week-old ICR female mice (Orient Bio) were utilized to create a mouse model of AS. Following an intraperitoneal injection of 240 mg/kg Avertin, a vertical incision in the abdominal wall was made to expose the uterus. At the utero-tubal junction, a small incision was created in each uterine horn, and each horn was traumatized in a standardized manner using a 27G needle (Korea vaccine, Ansan, Republic of Korea) entering through the lumen, rotated, and withdrawn 10 times.

Isolation of uterine cells

Uteri were dissected, minced into small pieces, and incubated in HBSS (Thermo) that contained Dispase and pancreatin for 1 h at 4°C and 1 h at room temperature. Tissues were incubated at 37°C for 10 min, then the supernatant (the epithelial cell-rich fraction) was collected. The remaining stromal cell-rich pellet was then digested with collagenase after filtration through a 70-μm nylon mesh. The cells were treated with fluorochrome-conjugated antibodies for 30 min at room temperature. Flow cytometry was used to examine cells after rinsing in washing buffer.

Hematoxylin and eosin staining

The uterus was dissected and then fixed in 4% PFA (BioPrince) for histology. After tissues were washed and dehydrated, they were embedded in paraplast (Leica Biosystems, Wetzlar, Germany). Paraffin-embedded tissues were sectioned using a microtome, stained with hematoxylin and eosin (H&E; Sigma-Aldrich), and observed by light microscopy (Carl Zeiss).

Hydroxyproline assay

The uterine tissues∼ (100 mg) were homogenized and added to 100 μL of 6 N concentrated NaOH. Tissue homogenate was heated at 120°C for 3 h for alkaline hydrolysis. The vial was allowed to cool briefly and then added to 100 μL of 6 N concentrated HCl to neutralize residual NaOH. The vial was centrifuged at 10,000 × *g* for 5 min, and supernatant was transferred to a new tube. The samples (20 μL) were prepared in a 96-well plate and incubated at 60°C for overnight. A total of 100 μL of citrate/acetate buffer was added at room temperature for 20 min and added to 100 μL of Ehrlich's solution at 60°C for 20 min. Absorbance was measured at optical density (OD) 560 nm on a microplate reader.

Statistical analysis

All values are reported as mean ± standard deviation (SD). For comparisons between two groups, the Mann-Whitney U test was used; for comparisons between more than two groups, the Kruskal-Wallis ANOVA test was used. A p value less than 0.05 was judged statistically significant. Statistical analysis was performed using GraphPad Prism v.8 software (GraphPad Software, La Jolla, CA, USA).

DATA AVAILABILITY

All data included in this study are available on request by contact with the corresponding author.

SUPPLEMENTAL INFORMATION

Supplemental information can be found online at https://doi.org/10.1016/j.omtn.2022.11.018.

ACKNOWLEDGMENTS

This research was supported by Basic Science Research Program through the National Research Foundation of Korea (NRF) funded by the Ministry of Education (NRF- 2019R1A6A1A03032888 to H.S. and NRF-2021R1A2C4001776 to W.P.), by the NRF grant funded by the Korea government (the Ministry of Science and ICT) (NRF-2020R1A2C2005012 to H.S. and NRF-2020R1A6A3A01100338 to M.P.), by Bio & Medical Technology Development Program of the NRF and funded by the Korean government (MSIT) (NRF-2022M3A9E4016936 to S.-H.H.), by a Korean Health Technology R&D Project grant through the Korea Health Industry Development Institute (KHIDI) funded by the Ministry of Health & Welfare, Republic of Korea (HI21C1353020021 to H.S.), and by the Korea Medical Device Development Fund grant funded by the Korea government (the Ministry of Science and ICT; the Ministry of Trade, Industry and Energy; the Ministry of Health & Welfare; and the Ministry of Food and Drug Safety) (NRF-2021M3E5E5096420 to W.P.). DC2.4 cells were kindly provided by K.L. Rock at the Dana-Farber Cancer Institute.

AUTHOR CONTRIBUTIONS

Conceptualization, M.P., H.-J.O., W.P., and H.S.; methodology, M.P., H.-J.O., J.H., and S.-H.H.; investigation, M.P., H.-J.O., and J.H.; writing – original draft, M.P., H.-J.O., J.H., W.P., and H.S.; funding acquisition, S.-H.H., W.P., and H.S.; supervision, W.P. and H.S.

DECLARATION OF INTERESTS

The authors declare no competing interests.

REFERENCES

1. Medzhitov, R. (2008). Origin and physiological roles of inflammation. Nature *454*, 428–435.
2. Nathan, C. (2002). Points of control in inflammation. Nature *420*, 846–852.
3. Kamaly, N., Fredman, G., Subramanian, M., Gadde, S., Pesic, A., Cheung, L., Fayad, Z.A., Langer, R., Tabas, I., and Farokhzad, O.C. (2013). Development and in vivo efficacy of targeted polymeric inflammation-resolving nanoparticles. Proc. Natl. Acad. Sci. USA *110*, 6506–6511.
4. Baardman, J., Verberk, S.G.S., Van der Velden, S., Gijbels, M.J.J., van Roomen, C.P.P.A., Sluimer, J.C., Broos, J.Y., Griffith, G.R., Prange, K.H.M., van Weeghel, M., et al. (2020). Macrophage ATP citrate lyase deficiency stabilizes atherosclerotic plaques. Nat. Commun. *11*, 6296–6315.
5. Hontecillas, R., Horne, W.T., Climent, M., Guri, A.J., Evans, C., Zhang, Y., Sobral, B.W., and Bassaganya-Riera, J. (2011). Immunoregulatory mechanisms of macrophage PPAR-γ in mice with experimental inflammatory bowel disease. Mucosal Immunol. *4*, 304–313.
6. Ma, Y., Yang, H., Zong, X., Wu, J., Ji, X., Liu, W., Yuan, P., Chen, X., Yang, C., Li, X., et al. (2021). Artificial M2 macrophages for disease-modifying osteoarthritis therapeutics. Biomaterials *274*, 120865.
7. Sahin Ersoy, G., Zolbin, M.M., Cosar, E., Moridi, I., Mamillapalli, R., and Taylor, H.S. (2017). CXCL12 promotes stem cell recruitment and uterine repair after injury in Asherman's syndrome. Mol. Ther. Methods Clin. Dev. *4*, 169–177.
8. Gargett, C.E., Nguyen, H.P.T., and Ye, L. (2012). Endometrial regeneration and endometrial stem/progenitor cells. Rev. Endocr. Metab. Disord. *13*, 235–251.
9. Conforti, A., Alviggi, C., Mollo, A., De Placido, G., and Magos, A. (2013). The management of Asherman syndrome: a review of literature. Reprod. Biol. Endocrinol. *11*, 118.
10. Park, M., Hong, S.H., Park, S.H., Kim, Y.S., Yang, S.C., Kim, H.R., Noh, S., Na, S., Lee, H.K., Lim, H.J., et al. (2020). Perivascular stem cell-derived cyclophilin A improves uterine environment with Asherman's syndrome via HIF1alpha-dependent angiogenesis. Mol. Ther. *28*, 1818–1832.
11. Lu, D., Xu, Y., Liu, Q., and Zhang, Q. (2021). Mesenchymal stem cell-macrophage crosstalk and maintenance of inflammatory microenvironment homeostasis. Front. Cell Dev. Biol. *9*, 681171.
12. Muñoz-Garcia, J., Cochonneau, D., Télétchéa, S., Moranton, E., Lanoe, D., Brion, R., Lézot, F., Heymann, M.F., and Heymann, D. (2021). The twin cytokines interleukin-34 and CSF-1: masterful conductors of macrophage homeostasis. Theranostics *11*, 1568–1593.
13. Martinez, F.O., and Gordon, S. (2014). The M1 and M2 paradigm of macrophage activation: time for reassessment. F1000Prime Rep. *6*, 13.
14. Liu, H., Wu, X., Gang, N., Wang, S., Deng, W., Zan, L., and Yu, S. (2015). Macrophage functional phenotype can be consecutively and reversibly shifted to adapt to microenvironmental changes. Int. J. Clin. Exp. Med. *8*, 3044–3053.
15. Yunna, C., Mengru, H., Lei, W., and Weidong, C. (2020). Macrophage M1/M2 polarization. Eur. J. Pharmacol. *877*, 173090.
16. Murray, P.J., and Wynn, T.A. (2011). Protective and pathogenic functions of macrophage subsets. Nat. Rev. Immunol. *11*, 723–737.
17. Chen, Z., Bozec, A., Ramming, A., and Schett, G. (2019). Anti-inflammatory and immune-regulatory cytokines in rheumatoid arthritis. Nat. Rev. Rheumatol. *15*, 9–17.
18. Zídek, Z., Anzenbacher, P., and Kmoníková, E. (2009). Current status and challenges of cytokine pharmacology. Br. J. Pharmacol. *157*, 342–361.
19. Gebert, L.F.R., and MacRae, I.J. (2019). Regulation of microRNA function in animals. Nat. Rev. Mol. Cell Biol. *20*, 21–37.
20. Tahamtan, A., Teymoori-Rad, M., Nakstad, B., and Salimi, V. (2018). Anti-inflammatory microRNAs and their potential for inflammatory diseases treatment. Front. Immunol. *9*, 1377.
21. Banerjee, S., Xie, N., Cui, H., Tan, Z., Yang, S., Icyuz, M., Abraham, E., and Liu, G. (2013). MicroRNA let-7c regulates macrophage polarization. J. Immunol. *190*, 6542–6549.
22. Lee, S.W.L., Paoletti, C., Campisi, M., Osaki, T., Adriani, G., Kamm, R.D., Mattu, C., and Chiono, V. (2019). MicroRNA delivery through nanoparticles. J. Contr. Release *313*, 80–95.
23. Miao, X., Leng, X., and Zhang, Q. (2017). The current state of nanoparticle-induced macrophage polarization and reprogramming research. Int. J. Mol. Sci. *18*, 336.
24. Kwon, D., Cha, B.G., Cho, Y., Min, J., Park, E.-B., Kang, S.-J., and Kim, J. (2017). Extra-large pore mesoporous silica nanoparticles for directing in vivo M2 macrophage polarization by delivering IL-4. Nano Lett. *17*, 2747–2756.
25. Huang, Y.-J., Hung, K.-C., Hung, H.-S., and Hsu, S-h (2018). Modulation of macrophage phenotype by biodegradable polyurethane nanoparticles: possible relation between macrophage polarization and immune response of nanoparticles. ACS Appl. Mater. Interfaces *10*, 19436–19448.
26. Wang, L., Zhang, H., Sun, L., Gao, W., Xiong, Y., Ma, A., Liu, X., Shen, L., Li, Q., and Yang, H. (2020). Manipulation of macrophage polarization by peptide-coated gold nanoparticles and its protective effects on acute lung injury. J. Nanobiotechnol. *18*, 1–16.
27. Raimondo, T.M., and Mooney, D.J. (2018). Functional muscle recovery with nanoparticle-directed M2 macrophage polarization in mice. Proc. Natl. Acad. Sci. USA *115*, 10648–10653.
28. Nguyen, M.-A., Wyatt, H., Susser, L., Geoffrion, M., Rasheed, A., Duchez, A.-C., Cottee, M.L., Afolayan, E., Farah, E., Kahiel, Z., et al. (2019). Delivery of microRNAs by chitosan nanoparticles to functionally alter macrophage cholesterol efflux in vitro and in vivo. ACS Nano *13*, 6491–6505.

29. Hillaireau, H., and Couvreur, P. (2009). Nanocarriers' entry into the cell: relevance to drug delivery. Cell. Mol. Life Sci. *66*, 2873–2896.

30. Zong, C., Xu, M., Xu, L.-J., Wei, T., Ma, X., Zheng, X.-S., Hu, R., and Ren, B. (2018). Surface-enhanced Raman spectroscopy for bioanalysis: reliability and challenges. Chem. Rev. *118*, 4946–4980.

31. van Rooijen, N., and Hendrikx, E. (2010). Liposomes for specific depletion of macrophages from organs and tissues. In Liposomes (Springer), pp. 189–203.

32. Moreno, S.G. (2018). Depleting macrophages in vivo with clodronate-liposomes. In Macrophages (Springer), pp. 259–262.

33. Shen, Z., Wichnieski, C., Carneiro, E., Garlet, G.P., Letra, A., and Silva, R.M. (2021). Expression profiling and functional characterization of MicroRNAs in apical periodontitis. J. Endod. *47*, 263–271.

34. Kamei, N., Yamamoto, S., Hashimoto, H., Nishii, M., Miyaura, M., Tomada, K., Nakase, I., and Takeda-Morishita, M. (2019). Optimization of the method for analyzing endocytosis of fluorescently tagged molecules: impact of incubation in the cell culture medium and cell surface wash with glycine-hydrochloric acid buffer. J. Contr. Release *310*, 127–140.

35. Cho, Y.K., Son, Y., Kim, S.-N., Song, H.-D., Kim, M., Park, J.-H., Jung, Y.-S., Ahn, S.-Y., Saha, A., Granneman, J.G., and Lee, Y.H. (2019). MicroRNA-10a-5p regulates macrophage polarization and promotes therapeutic adipose tissue remodeling. Mol. Metabol. *29*, 86–98.

36. Wei, Y., Zhu, M., and Schober, A. (2018). Macrophage microRNAs as therapeutic targets for atherosclerosis, metabolic syndrome, and cancer. Int. J. Mol. Sci. *19*, 1756.

37. Huang, X., Li, Y., Fu, M., and Xin, H.-B. (2018). Polarizing macrophages in vitro. In Macrophages (Springer), pp. 119–126.

38. Liu, Y.-C., Zou, X.-B., Chai, Y.-F., and Yao, Y.-M. (2014). Macrophage polarization in inflammatory diseases. Int. J. Biol. Sci. *10*, 520–529.

39. Park, M., Hong, S.-H., Park, S.H., Kim, Y.S., Yang, S.C., Kim, H.-R., Noh, S., Na, S., Lee, H.K., Lim, H.J., et al. (2020). Perivascular stem cell-derived Cyclophilin A improves uterine environment with Asherman's syndrome via HIF1α-dependent angiogenesis. Mol. Ther. *28*, 1818–1832.

40. Tu, Z., Chen, M., Wang, M., Shao, Z., Jiang, X., Wang, K., Yao, Z., Yang, S., Zhang, X., Gao, W., et al. (2021). Engineering bioactive M2 macrophage-polarized anti--inflammatory, antioxidant, and antibacterial scaffolds for rapid angiogenesis and diabetic wound repair. Adv. Funct. Mater. *31*, 2100924.

41. Han, J., Kim, Y.S., Lim, M.-Y., Kim, H.Y., Kong, S., Kang, M., Choo, Y.W., Jun, J.H., Ryu, S., Jeong, H-y, et al. (2018). Dual roles of graphene oxide to attenuate inflammation and elicit timely polarization of macrophage phenotypes for cardiac repair. ACS Nano *12*, 1959–1977.

42. Ganbold, T., and Baigude, H. (2018). Design of mannose-functionalized curdlan nanoparticles for macrophage-targeted siRNA delivery. ACS Appl. Mater. Interfaces *10*, 14463–14474.

43. Costa, A., Sarmento, B., and Seabra, V. (2018). Mannose-functionalized solid lipid nanoparticles are effective in targeting alveolar macrophages. Eur. J. Pharmaceut. Sci. *114*, 103–113.

44. Li, Y., Wu, H., Ji, B., Qian, W., Xia, S., Wang, L., Xu, Y., Chen, J., Yang, L., and Mao, H. (2020). Targeted Imaging of CD206 expressing tumor-associated M2-like macrophages using mannose-conjugated antibiofouling magnetic iron oxide nanoparticles. ACS Appl. Bio Mater. *3*, 4335–4347.

45. Pham, L.M., Kim, E.C., Ou, W., Phung, C.D., Nguyen, T.T., Pham, T.T., Poudel, K., Gautam, M., Nguyen, H.T., Jeong, J.H., et al. (2021). Targeting and clearance of senescent foamy macrophages and senescent endothelial cells by antibody-functionalized mesoporous silica nanoparticles for alleviating aorta atherosclerosis. Biomaterials *269*, 120677.

46. Chen, W.C., Kawasaki, N., Nycholat, C.M., Han, S., Pilotte, J., Crocker, P.R., and Paulson, J.C. (2012). Antigen delivery to macrophages using liposomal nanoparticles targeting sialoadhesin/CD169. PLoS One *7*, e39039.

47. He, H., Yuan, Q., Bie, J., Wallace, R.L., Yannie, P.J., Wang, J., Lancina, M.G., III, Zolotarskaya, O.Y., Korzun, W., Yang, H., and Ghosh, S. (2018). Development of mannose functionalized dendrimeric nanoparticles for targeted delivery to macrophages: use of this platform to modulate atherosclerosis. Transl. Res. *193*, 13–30.

48. Fang, Y., Shi, C., Manduchi, E., Civelek, M., and Davies, P.F. (2010). MicroRNA-10a regulation of proinflammatory phenotype in athero-susceptible endothelium in vivo and in vitro. Proc. Natl. Acad. Sci. USA *107*, 13450–13455.

49. Njock, M.-S., Cheng, H.S., Dang, L.T., Nazari-Jahantigh, M., Lau, A.C., Boudreau, E., Roufaiel, M., Cybulsky, M.I., Schober, A., and Fish, J.E. (2015). Endothelial cells suppress monocyte activation through secretion of extracellular vesicles containing antiinflammatory microRNAs. Blood *125*, 3202–3212.

50. Cheng, H.S., Sivachandran, N., Lau, A., Boudreau, E., Zhao, J.L., Baltimore, D., Delgado-Olguin, P., Cybulsky, M.I., and Fish, J.E. (2013). Micro RNA-146 represses endothelial activation by inhibiting pro-inflammatory pathways. EMBO Mol. Med. *5*, 1017–1034.

51. Bieber, T., Meissner, W., Kostin, S., Niemann, A., and Elsasser, H.-P. (2002). Intracellular route and transcriptional competence of polyethylenimine–DNA complexes. J. Contr. Release *82*, 441–454.

52. Yim, H., Park, W., Kim, D., Fahmy, T.M., and Na, K. (2014). A self-assembled polymeric micellar immunomodulator for cancer treatment based on cationic amphiphilic polymers. Biomaterials *35*, 9912–9919.

53. Hall, A., Lächelt, U., Bartek, J., Wagner, E., and Moghimi, S.M. (2017). Polyplex evolution: understanding biology, optimizing performance. Mol. Ther. *25*, 1476–1490.

54. Mellman, I., and Steinman, R.M. (2001). Dendritic cells: specialized and regulated antigen processing machines. Cell *106*, 255–258.

55. Patente, T.A., Pinho, M.P., Oliveira, A.A., Evangelista, G.C.M., Bergami-Santos, P.C., and Barbuto, J.A.M. (2018). Human dendritic cells: their heterogeneity and clinical application potential in cancer immunotherapy. Front. Immunol. *9*, 3176.

56. Park, J., Wu, C.T., and Bryers, J.D. (2013). Chemokine programming dendritic cell antigen response: part I - select chemokine programming of antigen uptake even after maturation. Immunology *139*, 72–87.

57. Singh, A., Talekar, M., Raikar, A., and Amiji, M. (2014). Macrophage-targeted delivery systems for nucleic acid therapy of inflammatory diseases. J. Contr. Release *190*, 515–530.

58. Wynn, T.A., and Ramalingam, T.R. (2012). Mechanisms of fibrosis: therapeutic translation for fibrotic disease. Nat. Med. *18*, 1028–1040.

59. Cao, Q., Harris, D.C.H., and Wang, Y. (2015). Macrophages in kidney injury, inflammation, and fibrosis. Physiology *30*, 183–194.

60. Liu, Y. (2011). Cellular and molecular mechanisms of renal fibrosis. Nat. Rev. Nephrol. *7*, 684–696.

61. Duffield, J.S. (2010). Macrophages and immunologic inflammation of the kidney. Semin. Nephrol. *30*, 234–254.

62. Braga, T.T., Agudelo, J.S.H., and Camara, N.O.S. (2015). Macrophages during the fibrotic process: M2 as friend and foe. Front. Immunol. *6*, 602.

63. Zhang, F., Ayaub, E.A., Wang, B., Puchulu-Campanella, E., Li, Y.H., Hettiarachchi, S.U., Lindeman, S.D., Luo, Q., Rout, S., Srinivasarao, M., et al. (2020). Reprogramming of profibrotic macrophages for treatment of bleomycin-induced pulmonary fibrosis. EMBO Mol. Med. *12*, e12034.

64. Kishore, A., and Petrek, M. (2021). Roles of macrophage polarization and macrophage-derived miRNAs in pulmonary fibrosis. Front. Immunol. *12*, 678457.

65. Thiruchelvam, U., Dransfield, I., Saunders, P.T.K., and Critchley, H.O.D. (2013). The importance of the macrophage within the human endometrium. J. Leukoc. Biol. *93*, 217–225.

66. Liu, D., Wang, J., Zhao, G., Jiang, P., Song, M., Ding, H., Wang, Z., Lv, H., and Hu, Y. (2020). CSF1-associated decrease in endometrial macrophages may contribute to Asherman's syndrome. Am. J. Reprod. Immunol. *83*, e13191.

67. Mao, R., Wang, C., Zhang, F., Zhao, M., Liu, S., Liao, G., Li, L., Chen, Y., Cheng, J., Liu, J., and Lu, Y. (2020). Peritoneal M2 macrophage transplantation as a potential cell therapy for enhancing renal repair in acute kidney injury. J. Cell Mol. Med. *24*, 3314–3327.

68. Piao, Y.J., Yoon, S.H., Kim, H.S., Moon, W.K., and Han, W. (2021). Application of immunotherapy based on dendritic cells stimulated by tumor cell-derived exosomes in a syngeneic breast tumor mouse model. Biochem. Biophys. Rep. *28*, 101136.

69. Huang, S., Wu, Y., Zhao, Z., Wu, B., Sun, K., Wang, H., Qin, L., Bai, F., Leng, Y., and Tang, W. (2021). A new mechanism of obeticholic acid on NASH treatment by inhibiting NLRP3 inflammasome activation in macrophage. Metabolism *120*, 154797.